
White Rose Research Online

eprints@whiterose.ac.uk
https://eprints.whiterose.ac.uk
Universities of Leeds, Sheffield and York

Deposited via The University of Leeds.

White Rose Research Online URL for this paper:
https://eprints.whiterose.ac.uk/id/eprint/87255/

Version: Published Version

Article:
Heath, GR (2014) Diffusion in low-dimensional lipid membranes. Nano letters, 14 (10). 5984 - 5988. ISSN: 1530-6984

https://doi.org/10.1021/nl503024v

Reuse
Items deposited in White Rose Research Online are protected by copyright, with all rights reserved unless indicated otherwise. They may be downloaded and/or printed for private study, or other acts as permitted by national copyright laws. The publisher or other rights holders may allow further reproduction and re-use of the full text version. This is indicated by the licence information on the White Rose Research Online record for the item.

Takedown
If you consider content in White Rose Research Online to be in breach of UK law, please notify us by emailing eprints@whiterose.ac.uk including the URL of the record and the reason for the withdrawal request.



NANO LETTERS

Letter

pubs.acs.org/NanoLett

Terms of Use CC-BY

Diffusion in Low-Dimensional Lipid Membranes

George R. Heath, Johannes Roth, Simon D. Connell, and Stephen D. Evans*

School of Physics and Astronomy, University of Leeds, Leeds LS2 9JT, United Kingdom

Supporting Information

ABSTRACT: The diffusion behavior of biological components in cellular membranes is vital to the function of cells. By collapsing the complexity of planar 2D membranes down to one dimension, fundamental investigations of bimolecular behavior become possible in one dimension. Here we develop lipid nanolithography methods to produce membranes, under fluid, with widths as low as 6 nm but extending to microns in length. We find reduced lipid mobility, as the width is reduced below 50 nm, suggesting different lipid packing in the vicinity of boundaries. The insertion of a membrane protein, M2, into these systems, allowed characterization of protein diffusion using high-speed AFM to demonstrate the first membrane protein 1D random walk. These quasi-1D lipid bilayers are ideal for testing and understanding fundamental concepts about the roles of dimensionality and size on physical properties of membranes from energy transfer to lipid packing.

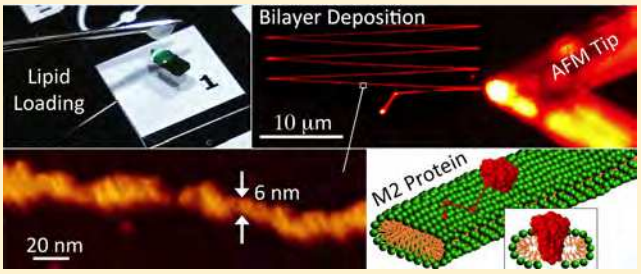

KEYWORDS: *Lipid membranes, high-speed AFM, nanolithography, molecular crowding, lipid diffusion*

Cell membranes provide complex and dynamic platforms for the organization of membrane components into functional assemblies to perform biologically important reactions. This makes membranes extremely attractive as platforms for bionanotechnology, and progress in the ability to reconstruct lipid membranes with biological functionality is highly sought after. Advances in supported lipid bilayer based membrane-mimicking systems have enabled a broad range of research from fundamental studies of intercellular signaling to biofuel cells.[1−6] To gain greater control and understanding of membrane components, we target the minimum size limit to the construction of free-standing supported lipid bilayers in one dimension. Lenhert et al. developed a dip-pen nanolithography method for patterning bilayer/multibilayers and were able to "write" bilayer patterns with feature sizes down to the micron level, under fluid, or to 100 nm under careful humidity in air.[7−9] Using an inverse "nanoshaving" technique, Cremer et al. etched 55 nm gaps into a BSA layer with an AFM tip and formed a lipid bilayer by backfilling these etched regions via vesicle fusion.[10] However, attempts to form lipid structures with dimensions less than 55 nm were unsuccessful, leading to the suggestion that they may have found the limit at which the smallest supported membranes could be produced, determined by the interplay between line tension and the work of adhesion.[10] Here we present a simple, highly reproducible tip based lithography approach that is able to produce stable supported lipid bilayers under fluid with feature sizes down to 6 nm. These ultralow dimensional membrane structures are created by priming AFM tips with a lipid coating, rinsing to remove excess lipid and then imaging the surface under fluid conditions (Figure 1A). Further it is possible to write single phase, fluid- or gel-phase, and multiphase bilayers (Figure S1). The formation of a biomimetic two-phase bilayer system formed from DOPC−sphingomyelin−cholesterol is shown in the Movie S1, and the phase separation into liquid ordered and liquid disordered domains is comparable to that observed for systems formed via vesicle fusion (Figure S1).

Inclusion of 2% Texas Red−DHPE lipid in the lipid mix allowed simultaneous visualization of the deposition process using fluorescence and AFM (Figure 1B) AFM images of DOPC bilayer stripes with heights of 4.5−5.5 nm and widths of 25 nm are shown in Figure 1C. The minimum continuous bilayer widths observed were 10 ± 2.5 nm wide (Figure 1D, E) as measured through the full-width-half-maximum, removing the tip convolution created by the 8 nm radius tip which gives a likely width of 6 ± 2.5 nm. The hydrophobic penalty associated with exposing the hydrophobic tails, at the edges of the bilayer, to water causes the bilayer to remodel into a hemimicellar configuration (Figure 1F).[11] For a 6−10 nm wide bilayer with ∼2.5 nm of lipid on either side taken up by the edges leaves only 1−5 nm wide regions of planar lipid; thus these systems are in the regime of tens of lipid molecules, or single membrane proteins, wide. Since a significant portion of the lipids are located in edge regions in these systems, this makes them ideal for studying lipid behavior at bilayer boundaries, which is crucial for understanding transient defects formed in cell membranes and hence for a range of important biological processes such as membrane fusion, endocytosis, viral infections, and budding.[12] The energy cost per unit length for reorganizing the lipids at the edge takes the form of edge tension (γ), while the interaction between the bilayer and the surface is given by the adhesion energy (W_A) and normally

Received: August 6, 2014
Revised: August 26, 2014
Published: August 28, 2014

 © 2014 American Chemical Society dx.doi.org/10.1021/nl503024v | *Nano Lett.* 2014, 14, 5984−5988

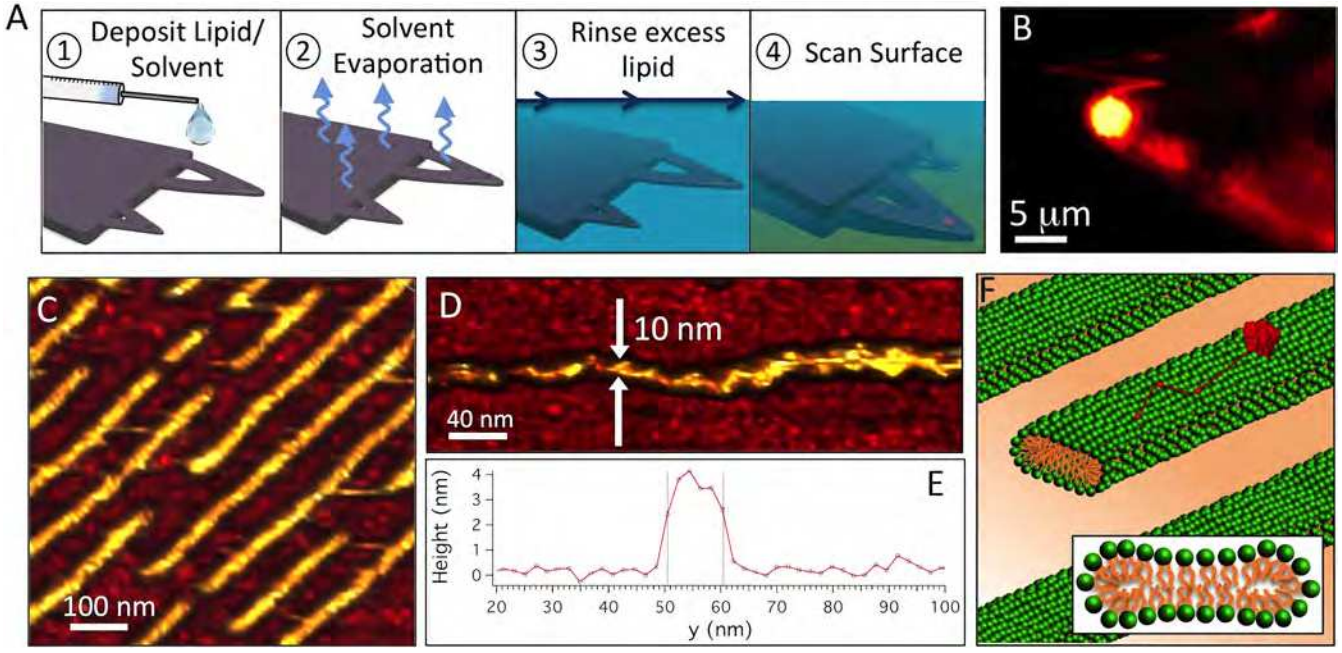

Figure 1. (A) Schematic of technique used to create 1D lipid bilayers: (1) lipid is deposited with a 5 μL droplet of lipid in chloroform, (2) the solvent is allowed to evaporate under vacuum, (3) excess lipid is removed from the back of the cantilever by submerging in water for 5 min, and (4) to write the lipid the surface is imaged under fluid conditions using contact mode. (B) False colored fluorescence image of in situ writing of DOPC−2% Texas Red DHPE lipid on mica. (C) AFM image of 25 nm wide DOPC bilayer stripes created by scanning a 25 μm area with 256 lines with a tip velocity of 50 μm/s. (D) AFM image of the minimum width DOPC bilayers created by scanning with a tip velocity of 100. (E) Height profile of dashed line in (D) showing the 10 nm width as measured by the full width half-maximum. (F) Schematic showing expected arrangement of lipids and proteins in 1D lipid bilayers.

more than counteracts penalty due to the line tension.[13] For bilayers of width, w, and length, l, these two energies can be equated to find the minimum stable bilayer dimensions:[10]

$$W_A \times w \times l = \gamma \times 2(w + l) \quad (1)$$

taking W_A to be 3.5×10^{-3} J/m^2 for PC vesicles adhering to mica[14] and γ to be 27.7 ± 2.5 pN.[15] For $l > 1$ μm eq 1 predicts a minimum for the value for w, for a stable DOPC bilayer bound to mica, to be around ∼15 nm, which is consistent with our observations.

Figure 2 shows that as tip speed, v, is increased, fewer lipids are deposited and the resulting bilayer stripes are narrower (see Supplementary Figure S2), thus providing fine control over stripe width between 10 and 200 nm. The relationship between w and v follows an inverse-square-root relation: $w = A/\sqrt{v}$, where A is a constant. This behavior suggests that the stripe width is kinetically controlled, i.e., governed the spreading of the bilayer on the surface. This has previously been shown to exhibit square-root-of-time dependence due to competition between a spreading power S and a resistive drag γ_s:[16−18]

$$w(t) = \sqrt{\frac{St}{2\gamma_s}} = \sqrt{\beta t} \quad (2)$$

taking a contact time of d/v, where d is the tip diameter, the spreading coefficient β can be determined from our fit in eq 2 to give a value of 6 μm^2/s, which is in reasonable agreement for PC lipids on mica.[16]

Lipid membranes are highly dynamic structures, and to function properly the lipids must be able to diffuse freely. Lipid mobility was determined using FRAP (fluorescence recovery after photobleaching) for lipid bilayer stripes of varying width. Figure 3A shows an example of images taken 10 s, 11 min, and

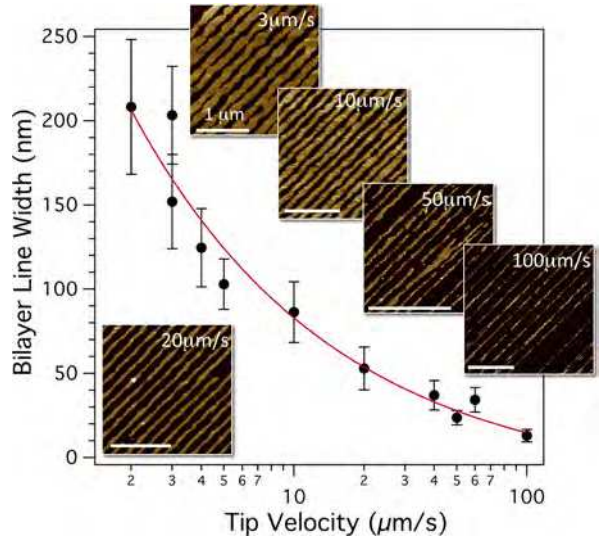

Figure 2. Control of bilayer stripe width via tip scan velocity for DOPC bilayers. The fit $w = 315.v^{-1/2}$ [inset: AFM images of bilayer stripes written by single tip trace per line at 3,10, 20, 50, and 100 μm/s (scale bars = 1 μm)].

24 min after bleaching an area of nanopatterned bilayer stripes (37 nm wide), shown schematically in Figure 3B. Analysis of the normalized fluorescence intensity curve vs time (Figure 3C) allows determination of the lipid diffusion coefficient and mobile fractions using the 1D diffusion equation (Figure 3D).[19] Finite element analysis simulations of bilayer recovery (Supplementary Figure S4) show the application of the 1D diffusion equation is valid when the bleach spot radius is significantly greater than the width of the bilayer stripe. Lipid

dx.doi.org/10.1021/nl503024v | Nano Lett. 2014, 14, 5984−5988

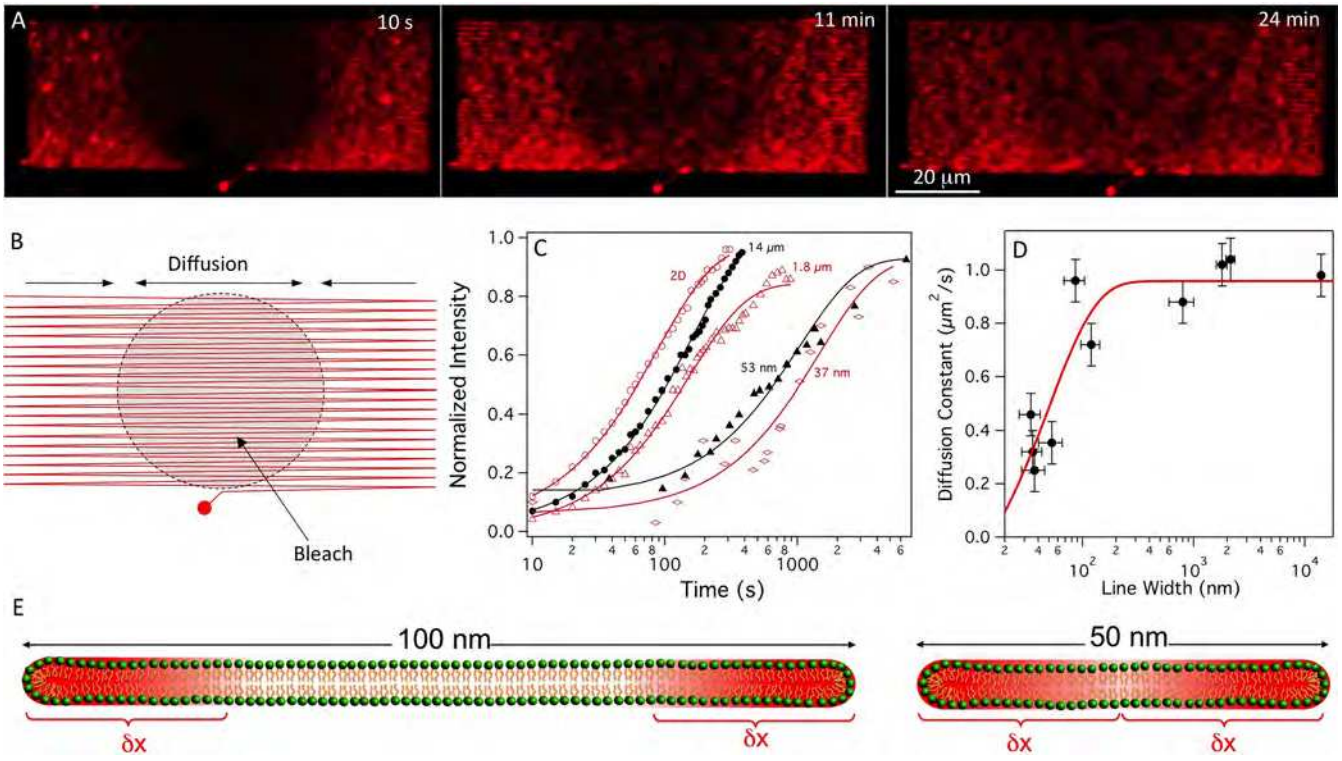

Figure 3. Diffusion behavior of lipids in nanoscopic bilayers. (A) FRAP images of multiple 2.0 mol % Texas red DHPE/DOPC bilayer stripes as a function of time with stripe widths of 37 ± 9 nm. The bleached bilayer spot is shown immediately after, at 11 min and at 24 min after bleaching (scale bars are 20 μm). (B) Schematic of the bleaching of zigzag bilayer stripes shown in (A). (C) Plots of normalized fluorescence intensity change of a bleached area, lines show fits used to determine diffusion constants and mobile fractions. (D) Diffusion constant as determined by the 1D diffusion equation as a function of bilayer line width. Additional images of varying line widths are shown in Figure S3. (E) Schematic representation showing the reduced mobility propagating a distance δx (~25 nm) from the bilayer edges leading to the decrease in diffusion constants observed below 100 nm.

molecules in stripes wider than 100 nm had an average diffusion coefficient of 0.95 ± 0.06 $\mu m^2/s$ (Figure 3E), in agreement with our own measurements of macroscopic 2D DOPC lipid bilayers (0.90 ± 0.10 $\mu m^2/s$) formed on mica. As the stripe width was decreased below 100 nm, the lipid mobility decreases sharply to values around 0.3 ± 0.1 $\mu m^2/s$ for bilayers with widths of ~35 nm. The mobile fraction varied in the range from 0.86 to 0.98 but showed no correlation with stripe width and with even the thinnest patterns typically giving 0.93. The decrease in diffusion coefficient with stripe width likely reflects the increase in bilayer fraction taken up by lipids, in the micellar caps, plus small fluctuations in bilayer width. The literature, based on both experiment and simulation, has been split over whether the lipid should be more "ordered" or "disordered" in these micellar caps, with perhaps a growing evidence that the presence of a membrane edge leads to higher density and reduced mobility.[11,20−22] How far this region of reduced mobility propagates into the bilayer has hitherto been undetermined. If the region of reduced mobility propagates a distance δx from the bilayer edge, then we would expect a dramatic reduction in mobility when the bilayer stripe width approaches $2\delta x$. Our results, Figure 3D, show that this reduced lipid mobility occurs for stripe widths less than 50 nm implying that the influence of the reduced mobility region extends for up to 25 nm from the bilayer edge (Figure 3E). Measurements of lipid bilayer height show that for decreasing bilayer width the height also decreases for widths less than 50 nm (Supplementary Figure S5). This decrease in height suggests conformational changes in lipid packing; however, typically we expect bilayers to increase in thickness with increased order and thus our data on decreasing height may suggest a tilted phase is induced at bilayer edges.

The controlled formation of bilayer stripes whose widths are sub 100 nm allows the investigation into effects of confinement on protein−lipid and protein−protein interactions, for integral and or peripheral membrane proteins. As a first demonstration of this, we have followed the insertion of the integral membrane protein M2, of the influenza virus that forms a pH sensitive proton channel in the viral lipid membrane and is essential for viral replication.[23] AFM height measurements of M2 in a supported lipid membrane show an average protrusion of 2 nm (Figure 4C) which is consistent with previous AFM in DPPC bilayers[24] and structural data.[23] High speed AFM scanning, at 0.25 frames per second, shows protein diffusion in bilayers of varying widths (Figure 4A, B and Supplementary Movies S2, S3). The typical step distance between frames range from 0 to 150 nm. $x-y$ displacement plots with time (Figure 4D, E) for the examples given in Supplementary Movies S2, S3 show that the M2 diffuses nonbiasedly along the thin bilayer stripes. Analysis of the mean squared displacement with time of the proteins gives 1D diffusion constants of 300 and 260 ± 30 nm^2/s for the 30 and 55 nm channels, respectively. The maximum velocities of the M2 protein, at 34 nm/s, are consistent with high-speed AFM data of other membrane proteins in 2D membranes.[25] Despite little difference in protein diffusion constant in the 2 different channel widths, it is clear to see in Figure 4D that the diffusion is confined within the central region of the bilayer stripes, supporting the idea that the lipid is

dx.doi.org/10.1021/nl503024v | Nano Lett. 2014, 14, 5984−5988

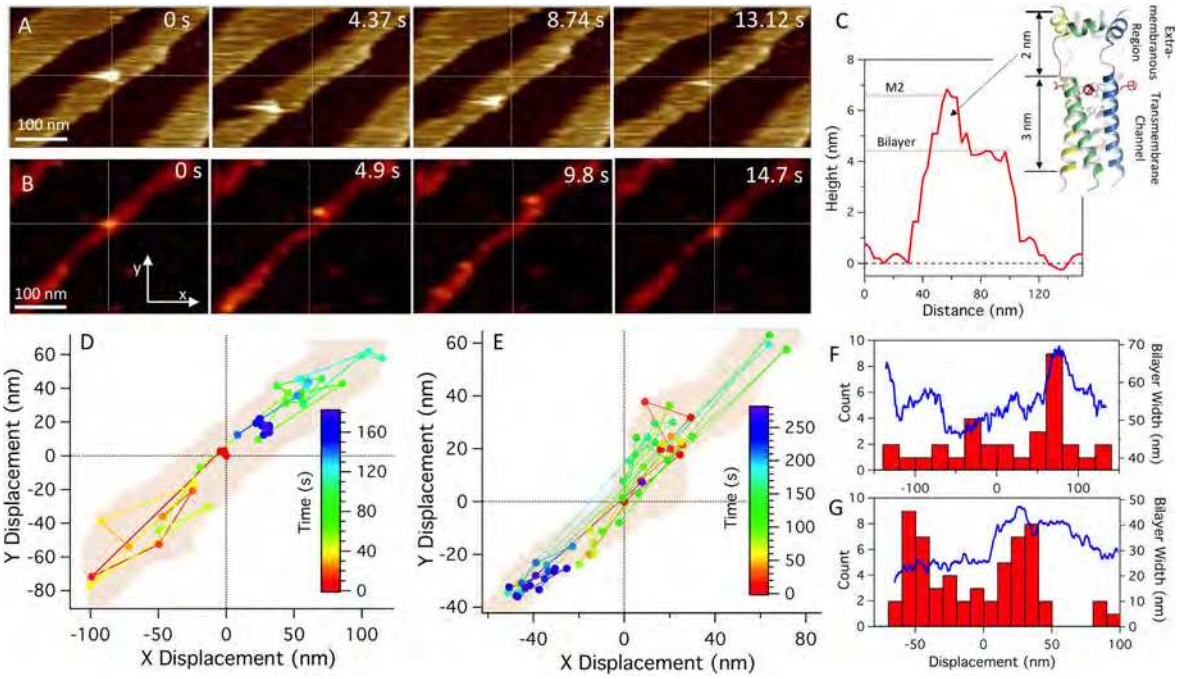

Figure 4. One-dimensional diffusion of the integral membrane protein M2 of influenza virus in 1D lipid bilayers. High-speed AFM image time sequences of M2 diffusion in 30 nm (A) and 60 nm (B) wide bilayer tracks (Supplementary Movies S1 and S2). (C) AFM height profile perpendicular to channel direction of M2 in a 60 nm wide channel. The structure of the M2 channel is shown with the four transmembrane helices and the amphipathic helices which protrude out of the membrane.[23] (D, E) Displacement traces of M2 protein in *x* and *y* relative to starting position analyzed from (A) and (B) respectively. (F, G) Combined histograms of protein displacement and line plot of bilayer width along the channel axis of (A, B), respectively.

more densely packed at the bilayer edge. Plots of displacement probability for a 1D random walk for purely random systems have a Gaussian profile. Figure 4F,G shows the displacement frequency along the channel axis. In the wider of the two channels (Figure 4F) the highest residency time is found in the widest parts of the channel, while the remaining regions generally obey Gaussian behavior about 0 displacement. In the thinner channel (Figure 4G) we find a double peaked distribution caused by the protein to becoming trapped in the thinnest region of the channel at −50 nm displacement. Figure 4G also shows the protein spends a large amount of time in the widest region of the channel due to lateral diffusion not in the channel direction.

In summary, we have shown a simple method forming stable patterned lipid membranes at length scales significantly less than previously observed and at the theoretically predicted limit for supported membrane stability. By measuring lipid diffusion in such patterned bilayers, we have shown that the lipid molecules undergo a sharp transition from 2D to 1D behavior as the pattern width reduces below 50 nm, suggesting that lipid ordering is different close to the edges of the bilayer patterns and that this ordering has an influence up to 25 nm from the bilayer edge. This has potential implications for pore/defect formation in membranes, processes that naturally occur in their vicinity, and for enhanced drug delivery using membrane poration techniques. Our data suggests that in the vicinity of the membrane edges the otherwise disordered lipids are in a more ordered, tilted, phase. Observation of the diffusion of the transmembrane protein, M2, in these nanopatterned bilayer stripes suggests there may be an optimum width of the mobile lipid region for enhanced diffusion. In 2D membranes (stripe width >100 nm) and in membranes of very restricted dimension (<25 nm) the directional diffusion of the protein is restricted for different reasons, either due to the dimensionality or due to the change in physical behavior of the lipids. Our work opens the way to watching biological processes on the scale of individual molecules, including conformation, chemistry, and organization. More importantly, it provides a model system for studying the role of dimensionality in biological processes, including photosynthesis, catalytic processes at membranes, and exchange of species between cells and their surroundings, in which the dynamic behavior of lipid membranes are key.

■ ASSOCIATED CONTENT

Ⓢ Supporting Information

Additional information including methods, experimental setups, AFM images of phase separated bilayers, AFM images showing varying line widths, fluorescence images showing FRAP of varying widths, finite element analysis simulations and bilayer height variations with width. Supporting videos of tip bilayer formation time lapse and M2 protein diffusion in 60 and 30 nm wide bilayers. This material is available free of charge via the Internet at http://pubs.acs.org.

■ AUTHOR INFORMATION

Corresponding Author

*E-mail: (S.D.E.) s.d.evans@leeds.ac.uk.

Author Contributions

G.R.H. and S.D.E. conceived the experiments. G.R.H. performed experiments. J.R. performed simulations. G.R.H., J.R., S.D.C., and S.D.E. analyzed the data and cowrote the paper.

Notes

The authors declare no competing financial interest.

■ ACKNOWLEDGMENTS

The authors thank Prof. Richard Bushby for critical discussion of the manuscript. The authors also thank Dr. Stephen Griffin for supplying the influenza M2 protein. This work was supported by the EPSRC, through grants EP/I000623/1 and EP/J017566.

■ REFERENCES

(1) Braun, T.; Ghatkesar, M. K.; Backmann, N.; Grange, W.; Boulanger, P.; Letellier, L.; Lang, H.-P.; Bietsch, A.; Gerber, C.; Hegner, M. *Nat. Nanotechnol.* **2009**, *4*, 179−185.
(2) Tanaka, M.; Sackmann, E. *Nature* **2005**, *437*, 656−663.
(3) Mossman, K. D. *Science* **2005**, *310*, 1191−1193.
(4) Liu, C.; Monson, C. F.; Yang, T.; Pace, H.; Cremer, P. S. *Anal. Chem.* **2011**, *83*, 7876−7880.
(5) Cheetham, M. R.; Bramble, J. P.; McMillan, D. G.; Krzeminski, L.; Han, X.; Johnson, B. R.; Bushby, R. J.; Olmsted, P. D.; Jeuken, L. J.; Marritt, S. J. *J. Am. Chem. Soc.* **2011**, *133*, 6521−6524.
(6) Radu, V.; Frielingsdorf, S.; Evans, S. D.; Lenz, O.; Jeuken, L. J. *J. Am. Chem. Soc.* **2014**, 8512−8515.
(7) Lenhert, S.; Mirkin, C. A.; Fuchs, H. *Scanning* **2010**, *32*, 15−23.
(8) Lenhert, S.; Sun, P.; Wang, Y.; Fuchs, H.; Mirkin, C. A. *Small* **2007**, *3*, 71−75.
(9) Lenhert, S.; Brinkmann, F.; Laue, T.; Walheim, S.; Vannahme, C.; Klinkhammer, S.; Xu, M.; Sekula, S.; Mappes, T.; Schimmel, T.; Fuchs, H. *Nat. Nanotechnol.* **2010**, *5*, 275−279.
(10) Shi, J.; Chen, J.; Cremer, P. S. *J. Am. Chem. Soc.* **2008**, *130*, 2718−2719.
(11) May, S. *Eur. Phys. J. E* **2000**, *3*, 37−44.
(12) Chernomordik, L. V.; Kozlov, M. M. *Annu. Rev. Biochem.* **2003**, *72*, 175−207.
(13) Lipowsky, R.; Seifert, U. *Mol. Cryst. Liq. Cryst.* **1991**, *202*, 17−25.
(14) Reviakine, I.; Brisson, A. *Langmuir* **2000**, *16*, 1806−1815.
(15) Portet, T.; Dimova, R. *Biophys. J.* **2010**, *99*, 3264−3273.
(16) Nissen, J.; Gritsch, S.; Wiegand, G.; Rädler, J. O. *Eur. Phys. J. B: Condens. Matter Complex Syst.* **1999**, *10*, 335−344.
(17) Sanii, B.; Parikh, A. N. *Soft Matter* **2007**, *3*, 974−977.
(18) Rädler, J.; Strey, H.; Sackmann, E. *Langmuir* **1995**, *11*, 4539−4548.
(19) Axelrod, D.; Koppel, D. E.; Schlessinger, J.; Elson, E.; Webb, W. W. *Biophys. J.* **1976**, *16*, 1055−1069.
(20) West, A.; Ma, K.; Chung, J. L.; Kindt, J. T. *J. Phys. Chem. A* **2013**, *117*, 7114−7123.
(21) Jiang, F. Y.; Bouret, Y.; Kindt, J. T. *Biophys. J.* **2004**, *87*, 182−192.
(22) Smith, A. M.; Vinchurkar, M.; Gronbech-Jensen, N.; Parikh, A. N. *J. Am. Chem. Soc.* **2010**, *132*, 9320−9327.
(23) Schnell, J. R.; Chou, J. J. *Nature* **2008**, *451*, 591−595.
(24) Hughes, T.; Strongin, B.; Gao, F. P.; Vijayvergiya, V.; Busath, D. D.; Davis, R. C. *Biophys. J.* **2004**, *87*, 311−322.
(25) Casuso, I.; Khao, J.; Chami, M.; Paul-Gilloteaux, P.; Husain, M.; Duneau, J.-P.; Stahlberg, H.; Sturgis, J. N.; Scheuring, S. *Nat. Nanotechnol.* **2012**, 1−5.